LETTER

doi:10.1038/nature09369

Water and its influence on the lithosphere–asthenosphere boundary

David H. Green[1,2], William O. Hibberson[2]*, István Kovács[2,3]* & Anja Rosenthal[2]*

The Earth has distinctive convective behaviour, described by the plate tectonics model, in which lateral motion of the oceanic lithosphere of basaltic crust and peridotitic uppermost mantle is decoupled from the underlying mechanically weaker upper mantle (asthenosphere). The reason for differentiation at the lithosphere–asthenosphere boundary is currently being debated with relevant observations from geophysics (including seismology) and geochemistry (including experimental petrology). Water is thought to have an important effect on mantle rheology, either by weakening the crystal structure of olivine and pyroxenes by dilute solid solution[1], or by causing low-temperature partial melting[2]. Here we present a novel experimental approach to clarify the role of water in the uppermost mantle at pressures up to 6 GPa, equivalent to a depth of 190 km. We found that for lherzolite in which a water-rich vapour is present, the temperature at which a silicate melt first appears (the vapour-saturated solidus) increases from a minimum of 970 °C at 1.5 GPa to 1,350 °C at 6 GPa. We have measured the water content in lherzolite to be approximately 180 parts per million, retained in nominally anhydrous minerals at 2.5 and 4 GPa at temperatures above and below the vapour-saturated solidus. The hydrous mineral pargasite is the main water-storage site in the uppermost mantle, and the instability of pargasite at pressures greater than 3 GPa (equivalent to more than about 90 km depth) causes a sharp drop in both the water-storage capacity and the solidus temperature of fertile upper-mantle lherzolite. The presence of interstitial melt in mantle with more than 180 parts per million of water at pressures greater than 3 GPa alters mantle rheology and defines the lithosphere–asthenosphere boundary. Modern asthenospheric mantle acting as the source for mid-oceanic ridge basalts has a water content of 50–200 parts per million (refs 3–5). We show that this matches the water content of residual nominally anhydrous minerals after incipient melting of lherzolite at the vapour-saturated solidus at high pressure.

The Earth's upper mantle is mainly of lherzolite composition, and evidence from magmas and mantle xenoliths reveals the importance of small amounts of key volatile components (H_2O, CO_2 and CH_4—that is, C–H–O—and to a lesser extent F, Cl and S) in controlling the solidus temperature and subsolidus mineralogy in the upper mantle. Water is the main volatile component and is present in trace amounts (less than 0.2 wt%) in mid-ocean-ridge parental magmas at divergent plate boundaries[3,4]; is recycled into the mantle in subduction zones; and is a significant component (more than 1 wt%) of parental magmas at convergent margins[5]. The melting relationships of lherzolite + (C–H–O) are particularly applicable to the genesis of intra-plate basalts (rift and hotspot) and arc basalts (including boninites, arc tholeiites and ankaramites), which have significant water and carbon dioxide contents[2,6–10].

Despite this, the petrogenesis of mid-ocean-ridge basalts (MORBs) has been addressed by the study of the melting of lherzolite in the absence of significant amounts of carbon or water in mantle source regions. This is justified by the observation that the most primitive MORBs have approximately 0.1% H_2O and 100 parts per million (p.p.m.) CO_2, which depress liquidus temperatures by less than 30 °C and do not alter liquidus phase relationships significantly[2,4]. Translating these water contents to the basalt source region by assuming 5–20% melting to produce MORBs gives estimates of upper-mantle water contents of 50–200 p.p.m. It has been argued that at this concentration water behaves as a trace component in nominally anhydrous minerals (NAMs); its effect on solidus temperatures is uncertain at very low concentrations[1,9–13]. The presence or absence of partial melting in the upper mantle significantly affects seismological and rheological properties, and must be understood to enable us to address first-order geodynamic models[2,8,14–16].

A pivotal constraint for upper-mantle models is the 'water-saturated solidus'[6,8–10]: the vapour-saturated solidus for water-rich vapour. Recently, an experimental study[15] placed the 'water-saturated solidus' at temperatures 200–400 °C lower than those indicated by earlier work[8,16,17] at pressures of 3–5 GPa. The same study found that pargasite was unstable at the vapour-saturated solidus at 2 GPa, whereas earlier studies[8,16,17] found pargasite up to 3 GPa. Our study clarifies these interpretations by varying bulk water content at 2.5 GPa with examination of equilibrium phase compositions, and identification of quench material as derived from either melt or vapour[18]. The novelty of our approach includes the use of olivine disks or monomineralic layers as melt and vapour-phase traps. The monomineralic layers also act as sensor layers for the use of Fourier transform infrared (FTIR) spectroscopy for measurements of H_2O (that is, OH^-) in NAMs (that is, olivine and pyroxenes) under conditions in which the roles of hydrous mineral stability, partial melting or vapour-saturation were also monitored[8,15–17] (Supplementary Fig. 1). We used low water contents, mainly 1.45 and 0.145 wt% H_2O, to avoid the leaching of low-melting components by excessive water (14.5 wt%)[15]. We determined the vapour-saturated solidus at pressures up to 6 GPa (Fig. 1, Supplementary Figs 1 and 2).

At 2.5 GPa, 1,000 °C, experiments with high (7.25 and 14.5 wt%) water content (as in ref. 15) do not contain pargasite. Clinopyroxene has less than 0.2 wt% Na_2O, and samples contain common glass films and 'froth' coating euhedral minerals, with abundant void space. The observed assemblage is quenched from lherzolitic NAMs (that is, olivine, pyroxenes and garnet) and the water-rich vapour phase. Our data are consistent with data from ref. 15 at 2.4 GPa with 14.5 wt% H_2O, in that experiments at 1,100 °C and 900 °C do not contain pargasite and have more than 10% clinopyroxene, with 0.07 and 0.26 wt% Na_2O respectively. Although ref. 15 interprets experiments from 880 °C to 1,100 °C as containing hydrous silicate melt, our larger experimental study clarifies the phase relationships (Fig. 2) and identifies vapour-phase quench. The experiments[15] also constrain the disappearance of clinopyroxene by melting reactions (Fig. 2) to be above 1,100 °C, appropriate for the refractory, vapour-leached minerals in equilibrium with water-rich vapour.

[1]School of Earth Sciences and Centre for Ore Deposit Studies, University of Tasmania, Hobart 7001, Tasmania, Australia. [2]Research School of Earth Sciences, The Australian National University, Mills Road, Canberra, Australian Capital Territory 0200, Australia. [3]Department of Data Management, Eötvös Loránd Geophysical Institute of Hungary, Columbus utca 17–23, H-1145 Budapest, Hungary.
*These authors contributed equally to this work.

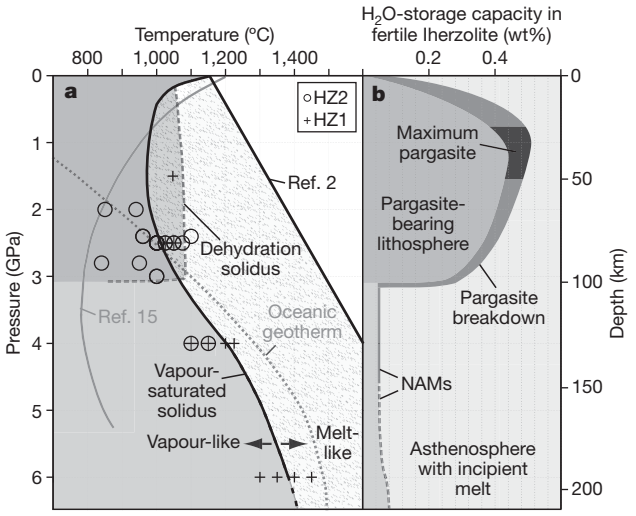

Figure 1 | The vapour-saturated solidus and the water-storage capacity of HZ1 lherzolite. **a**, The experimental determination of the vapour-saturated solidus of HZ1 lherzolite composition. The solidus is consistent with earlier work[2,8,16,17], and our experimental study shows that the inference of much lower solidus temperatures[15] (as illustrated) results from misinterpretation of vapour-phase quench as quenched silicate melt[16–18]. The dehydration solidus[8,16,17]—the solidus for pargasite lherzolite without excess water—is also shown, as is a schematic oceanic geotherm which passes through the dehydration solidus at about 90 km, 1,070 °C. **b**, The experimentally determined water-storage capacity of HZ1 lherzolite along the solidus to more than 4 GPa. We illustrate the sharp reduction in water-storage capacity along the solidus from high values (to 0.5 wt%) in the uppermost mantle, where pargasite is stable, to much lower capacities (approximately 0.02 wt%) in NAMs at 3–4 GPa.

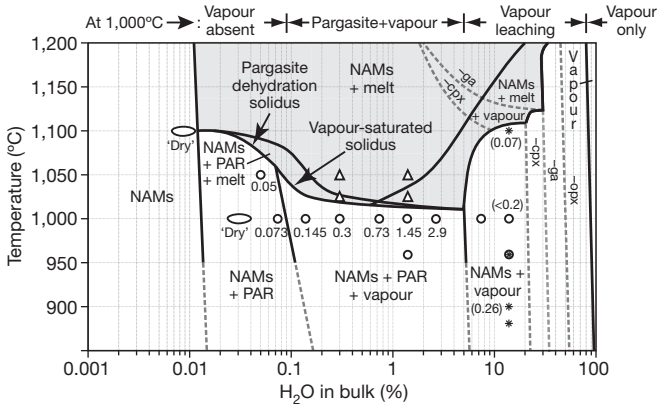

Figure 2 | Phase stability fields with different water contents in HZ1 and HZ2 lherzolite compositions at 2.5 GPa. Note logarithmic scale for water content. Referring to the sequence of experiments at 2.5 GPa, 1,000 °C, vapour is absent at less than 0.1 wt% H_2O (water is held in NAMs or NAMs + pargasite) and pargasite is unstable at more than 5 wt% H_2O, owing to dissolution of Na_2O and K_2O (essential for pargasite stability) in the increasingly water-rich vapour phase. At high water/rock ratios (more than 5 wt% H_2O), lherzolite HZ1 is composed of refractory NAMs and is leached of low-melting components by the vapour phase. It does not experience melting at low temperatures and may be leached by very large water/rock ratios to residual dunite + vapour[18,28]. Open circle and open ellipse, subsolidus; open triangle, hydrous silicate melt present; asterisk, experiments at 2.4 GPa from ref. 15; light grey shaded area, presence of melt. PAR, pargasite; ga, garnet; cpx, clinopyroxene; opx, orthopyroxene.

Experiments with lower water content (for example, 1.45 wt% H_2O), contain stable pargasite (3.4 wt% Na_2O, 0.4 wt% K_2O) and clinopyroxene (1.0 wt% Na_2O), and have lower porosity. At a slightly higher temperature, the presence of hydrous silicate melt of olivine-rich basanite to nephelinite composition at 2.5 GPa, 1,025 °C is readily identified by silicate quench minerals in intersertal texture in the olivine melt trap layers. By varying the temperature and water content at 2.5 GPa, we defined the phase fields for pargasite, silicate melt and aqueous vapour (Fig. 2, Supplementary Tables 3 and 4). The new data confirm the importance of pargasite as a hydrous phase stable up to the lherzolite solidus in the upper 90–100 km of the mantle[8,16,17]. Phase assemblages at high water contents (greater than 5 wt% approximately) may be inferred from earlier high-pressure studies of olivine-rich basalts and of peridotite with varying water contents[19–24]. Assemblages become increasingly refractory with successive elimination of clinopyroxene, garnet and orthopyroxene, as less-refractory components are partitioned into the aqueous vapour phase. Consequently, the appearance of hydrous silicate melt (containing approximately 30 wt% H_2O at 2.5 GPa) in the system is displaced to higher temperatures as the water/rock ratio increases. The appearance of 'vapour + melt' fields with residual NAMs is inferred from earlier studies at 2–3 GPa, in which the maximum water content and liquidus depression for olivine-rich melts were demonstrated to be 25–30 wt% H_2O (refs 20–24). The lherzolite + water system does not display supercritical behaviour at 2.5 GPa (refs 8, 22 and 23).

We also investigated the vapour-saturated solidus for HZ1 lherzolite (an estimate of the composition of the source for MORBs) at 4 GPa, 1,210 °C, and at 6 GPa, 1,350 °C, using olivine layers as melt traps and for measurement of the water contents of NAMs. At 4 GPa there is clear distinction between subsolidus, vapour-bearing experiments and those with quenched hydrous silicate melt, and supercritical behaviour is not observed. However, at 6 GPa the subsolidus water-rich vapour has a high solute content, and the compositional separation between hydrous silicate melt and water-rich vapour seems to be less than at lower pressure. Supercritical behaviour is possible at this pressure[23,24].

We have also determined, using FTIR spectroscopy[25–27], the water contents of olivine, orthopyroxene and clinopyroxene co-existing with pargasite below the water-saturated solidus, and co-existing with hydrous silicate melt above the solidus (Fig. 3, Supplementary Tables 3 and 4). The experimental data provide water-partitioning coefficients between NAMs, pargasite and phlogopite, and hydrous silicate melt at 2.5 and 4 GPa. A maximum of approximately 180 p.p.m. H_2O is partitioned into residual NAMs in the presence of melt at the vapour-saturated solidus at 2.5 GPa, 1,025 °C, and 4 GPa, 1,210 °C. FTIR measurements on olivine and pyroxene layers showed more water in olivine and less water in pyroxenes at 4 GPa than at 2.5 GPa, with the net result that residual lherzolite at the water-saturated solidus contains approximately 180 p.p.m. H_2O at both 2.5 and 4 GPa in NAMs, within experimental uncertainty.

Water-storage capacity (the maximum amount of structurally bound water in mantle minerals before the appearance of an aqueous vapour phase or hydrous silicate melt) in the uppermost mantle is dominated by pargasite and has a maximum of about 0.6 wt% H_2O (30% pargasite) at about 1.5 GPa, decreasing to about 0.2 wt% H_2O (10% pargasite) at 2.5 GPa. The decrease is caused by the changing composition of pargasite in lherzolite as a function of pressure[17]. At pressures greater than 3 GPa pargasite is no longer stable in fertile lherzolite, so the water-storage capacity of fertile lherzolite drops abruptly to approximately 180 p.p.m.; that is, fertile lherzolite with more than 180 p.p.m. H_2O contains a water-rich vapour phase at greater than 3 GPa and undergoes melting at the vapour-saturated solidus. The behaviour of lherzolite + H_2O is also strongly dependent on the water/rock ratio. Experiments at 2.5 GPa with water contents varying from 'dry' to 14.5 wt% H_2O demonstrate that the increasingly water-rich vapour phase leaches oxides, particularly K_2O and Na_2O, from the crystalline phases. Also, if more than 5 wt% H_2O is present at 2.5 GPa, pargasite is absent and the residual lherzolite minerals contain no Na, K or other low-melting components. The vapour-saturated solidus for this refractory assemblage is at a higher temperature[19], as shown by the persistence of clinopyroxene at 1,100 °C, 14.5 wt% H_2O (ref. 15). The aqueous vapour phase changes continuously with increasing solute content, notably leaching alkalis and silica from the

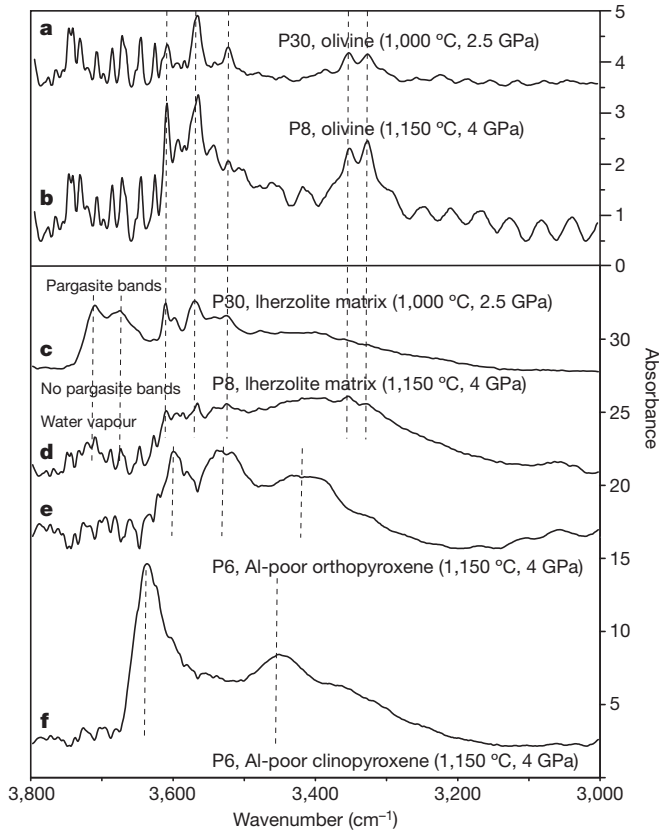

Figure 3 | Examples of FTIR spectra from lherzolite layer or from monomineralic olivine or pyroxene layers. The spectra are normalized to 1 cm of thickness. Calibrations of spectra to derive water content, summarized in the text, are based on refs 25–27. The spectra from monomineralic layers were used for quantitative estimation of their water content, whereas those of the lherzolite matrix were only used for monitoring the presence and absence of hydrous phases (pargasite and phlogopite), also analysed by electron microprobe. Experiment P30, HZ1 lherzolite composition at 2.5 GPa, 1,000 °C, dry (that is, no H_2O added); experiment P6, HZ1 lherzolite composition at 4 GPa, 1,150 °C, 1.45 wt% H_2O; experiment P8, 95% HZ1 lherzolite + 5% 'anhydrous phlogopite' at 4 GPa, 1,150 °C, 1.45 wt% H_2O.

lherzolite. This initially destabilizes pargasite, as we have shown, but with even higher water/rock ratios, it also destabilizes clinopyroxene and garnet, followed by orthopyroxene, to yield olivine + vapour at sufficiently high water/rock ratios. The vapour-saturated solidi for these increasingly refractory mineral assemblages move to higher temperatures, as shown schematically in Fig. 2. The experiments demonstrate a leaching process at very high water/rock ratios, which may be significant in the intermittent, channelled flow of vapour or melt + vapour, resulting in dunite channels through lherzolite[18,28].

The confirmation that the high-pressure limit of pargasite stability in fertile lherzolite is 3 GPa at 1,000–1,100 °C is of prime importance in understanding the lithosphere–asthenosphere character of the uppermost mantle[2,8–10,13–17]. Pargasite stability along continental and oceanic geotherms to depths of about 90 km, and its instability at deeper levels, causes a sharp reduction in the water-storage capacity of upper-mantle minerals. An appropriate geotherm passes from subsolidus mineralogy, in which neither aqueous vapour nor hydrous melt are present and water is contained within pargasite and NAMs, to an assemblage in which a small melt fraction coexists with NAMs containing approximately 180 p.p.m. H_2O (Fig. 1). The melt composition is that of olivine nephelinite containing about 30 wt% H_2O (refs 20–24), and the degree of melting or melt fraction is thus determined by the bulk water content of mantle lherzolite: that is, about 1% melt for 0.3 wt% H_2O. The transition from subsolidus lherzolite to lherzolite with a very small melt fraction has a significant effect on mantle rheology[29]. Recent work demonstrates that the melt weakens and the strain rate increases by two orders of magnitude from melt-free (but not 'dry' in the sense of water-absent) dunite to dunite with a very small silicate melt fraction[29]. Thus it is argued that a major change in rheology occurs beneath the oceanic lithosphere at depths of about 90 km. If the water content of the mantle is greater than 180 p.p.m. in the depth range of about 90–190 km, intraplate oceanic geotherms traverse a region of 'incipient melting'. The melt fraction, probably less than 1%, is controlled by the water content, and the melt movement is retarded by low permeability for porosities of less than 1–2% melt fraction[30]. If the very small melt fraction migrates upwards along the geotherm, it will react with lherzolite or harzburgite, and will crystallize pargasite at less than 3 GPa (refs 8,16,17). The asthenosphere at depths greater than 90 km is thus a region in which deeper levels become depleted of components that partition strongly into a hydrous silicate melt relative to garnet lherzolite. Our experimental data show that water partition coefficients are $D_{\mathrm{melt/peridotite}} \approx 1.6 \times 10^3$, based on a water content of about 30 wt% in near-solidus melt at more than 3 GPa, 1,025 °C, and about 180 p.p.m. H_2O in residual garnet lherzolite (NAMs).

It is not a coincidence that the source regions for parental MORBs have less than 200 p.p.m. H_2O; rather, this is consistent with the residual water in NAMs after melt loss at or near the vapour-saturated solidus. By this process, deeper levels of the asthenosphere (MORB source) are depleted, possibly in a continuous process associated with mantle degassing, by slow migration of a very small melt fraction[7]. The upper levels of the asthenosphere are enriched by this migration and acquire the trace-element characteristics of enriched MORBs and intraplate basalts. The stability of pargasite at less than 3 GPa limits the ascent of incipient melt, and the base of the lithosphere is enriched over time by crystallization of pargasite and, for higher K/Na compositions, also of phlogopite. Water is not only important in causing the rheological contrast between the lithosphere and the asthenosphere in intraplate settings, but it also has a significant role at convergent margins. Geophysical modelling of the subduction of ocean crust predicts distinctive inversion of temperature–depth profiles in the mantle wedge above the seismic Benioff zone. Progressive dehydration of oceanic crust and uppermost mantle lithologies enables transport of water, either as vapour (H_2O-dominated C–O–H–S vapour) or as water-rich silicate melt, into the mantle wedge. The mantle wedge above the subducting oceanic lithosphere is generally inferred to be the location in modern geodynamics in which water has a major influence on rheology, volcanism and seismicity. Our new data show that melting of lherzolite at or near the vapour-saturated solidus in the slab–wedge environment does not dehydrate residual harzburgite, but that residual lithosphere returned to the upper mantle may carry approximately 180 p.p.m. H_2O. Modelling of subduction-related melting or of vapour-phase transport must be based on the correct location of the vapour-saturated solidus of lherzolite[2,8,16,17].

Table 1 | Model mantle compositions (wt%) used in experimental study of vapour-saturated lherzolite solidus to 6 GPa.

Starting composition	SiO_2	TiO_2	Al_2O_3	Cr_2O_3	FeO	MnO	MgO	CaO	Na_2O	K_2O	NiO	Total	Mg#
HZ1 (H&Z lherzolite)[15]	46.20	0.18	4.08	0.40	7.59	0.10	37.96	3.23	0.33	0.03	0.28	100.2	89.9
HZ2 (Fe-depleted H&Z lherzolite)	46.84	0.19	4.28	0.42	4.14	0.10	39.80	3.39	0.35	0.03	0.29	99.8	94.5
MPY (MOR pyrolite)[2,17]	44.74	0.17	4.37	0.45	7.55	0.11	38.57	3.38	0.40	0.00	0.26	100.0	90.1

HZ1 and mid-ocean-ridge pyrolite are estimates of the upper-mantle composition in the region acting as the source for MORBs, namely, the asthenosphere.

METHODS SUMMARY

The lherzolite composition HZ1 (ref. 15) is an estimate of the composition of the source for MORBs, and is very close to mid-ocean-ridge pyrolite[2], except that HZ1 contains 0.03 wt% K_2O (Table 1). We placed a layer of lherzolite with known water content between two 'sensor' layers of olivine, of orthopyroxene and clinopyroxene, or of olivine and orthopyroxene, sealed within Au, Ag or AuPd capsules. We ran capsules at 1.5, 2.5, 3, 4 and 6 GPa in modified piston-cylinder apparatuses for long times and at temperatures below and above the water-saturated solidus. We sectioned and polished the capsules, and determined phase compositions in the lherzolite and sensor layers by energy-dispersive X-ray microanalysis. We used doubly polished sections of 37–124 μm thickness to obtain FTIR absorption spectra. FTIR spectra from the lherzolite layers showed the presence or absence of pargasite and phlogopite, confirmed by microprobe analyses. The characteristic absorption peaks for structurally bound water in mineral phases enabled quantitative estimations of water contents, using the unpolarized infrared method of ref. 25 and the calibrations of refs 26 and 27. In seeking to reconcile recent determination of the 'water-saturated solidus' with earlier work, varying water content was an important step. Following ref. 15, we prepared HZ1 containing 14.5 wt% H_2O with all MgO added as $Mg(OH)_2$, together with a second anhydrous mix. We mixed these two compositions in appropriate proportions to give 100 mg batches with 0.073 to 7.25 wt% H_2O (Fig. 2). We also prepared samples with low water content by synthesizing pargasite lherzolite[17]. The systematic behaviour of K_2O in pargasite or in melt or vapour phase, and of Na_2O in pargasite, clinopyroxene, melt or vapour, illustrates the effectiveness of the methods used to control water.

Full Methods and any associated references are available in the online version of the paper at www.nature.com/nature.

Received 4 February; accepted 22 July 2010.

1. Hirth, G. & Kohlstedt, D. L. Water in the oceanic upper mantle: implications for rheology, melt extraction and the evolution of the lithosphere. *Earth Planet. Sci. Lett.* **144,** 93–108 (1996).
2. Green, D. H. & Falloon, T. J. in *The Earth's Mantle* (ed. Jackson, I.) 311–378 (Cambridge Univ. Press, 1998).
3. Michael, P. J. Regionally distinctive sources of depleted MORB: evidence from trace elements and H_2O. *Earth Planet. Sci. Lett.* **170,** 215–239 (1995).
4. Danyushevsky, L. V., Eggins, S. M., Falloon, T. J. & Christie, D. M. H_2O abundance in depleted to moderately enriched mid-ocean ridge magmas; Part I: incompatible behaviour, implications for mantle storage, and origin of regional variations. *J. Petrol.* **41,** 1329–1364 (2000).
5. Sobolev, A. V. & Chaussidon, M. H_2O concentrations in primary melts from supra-subduction zones and mid-ocean ridges: implications for water storage and recycling in the mantle. *Earth Planet. Sci. Lett.* **137,** 45–55 (1996).
6. Wyllie, P. J. Mantle fluid compositions buffered in peridotite–CO_2–H_2O by carbonates, amphibole, and phlogopite. *J. Geol.* **86,** 687–713 (1978).
7. Green, D. H. Compositions of basaltic magmas as indicators of conditions of origin: application to oceanic volcanism. *Phil. Trans. R. Soc. Lond. A* **268,** 707–725 (1971).
8. Green, D. H. Experimental melting studies on a model upper mantle composition at high pressures under water-saturated and water-undersaturated conditions. *Earth Planet. Sci. Lett.* **19,** 37–53 (1973).
9. Hirschmann, M. M. Water, melting, and the deep Earth H_2O cycle. *Annu. Rev. Earth Planet. Sci.* **34,** 629–653 (2006).
10. Asimow, P. D., Dixon, J. E. & Langmuir, C. H. A hydrous melting and fractionation model for mid-ocean ridge basalts: application to the Mid-Atlantic Ridge near the Azores. *Geochem. Geophys. Geosyst.* **5,** 1–24 (2004).
11. Tenner, T. J., Hirschmann, M. M., Withers, A. C. & Hervig, R. L. Hydrogen partitioning between nominally anhydrous upper mantle minerals and melt between 3 and 5 GPa and applications to hydrous peridotite partial melting. *Chem. Geol.* **262,** 42–56 (2009).
12. McKenzie, D. & Bickle, M. J. The volume and composition of melt generated by extension of the lithosphere. *J. Petrol.* **29,** 625–679 (1988).
13. Artemieva, I. M. The continental lithosphere: reconciling thermal, seismic and petrologic data. *Lithos* **109,** 23–44 (2009).
14. Thybo, H. The heterogeneous upper mantle low velocity zone. *Tectonophysics* **416,** 53–79 (2006).
15. Grove, T. L., Chatterjee, N., Parman, S. W. & Medard, E. The influence of H_2O on mantle wedge melting. *Earth Planet. Sci. Lett.* **249,** 74–89 (2006).
16. Milhollen, G., Irving, A. J. & Wyllie, P. J. Melting interval of peridotite with 5.7 per cent water to 30 kilobars. *J. Geol.* **82,** 575–587 (1974).
17. Niida, K. & Green, D. H. Stability and chemical composition of pargasitic amphibole in MORB pyrolite under upper mantle conditions. *Contrib. Mineral. Petrol.* **135,** 18–40 (1999).
18. Bowen, N. L. & Tuttle, O. F. The system MgO–SiO_2–H_2O. *Bull. Geol. Soc. Am.* **60,** 439–460 (1949).
19. Asahara, Y. & Ohtani, E. Melting relations of the hydrous primitive mantle in the CMAS–H_2O system at high pressures and temperatures, and implications for the generation of komatiites. *Phys. Earth Planet. Inter.* **125,** 31–44 (2001).
20. Green, D. H. Conditions of melting of basanite magma from garnet peridotite. *Earth Planet. Sci. Lett.* **17,** 456–465 (1973).
21. Brey, G. & Green, D. H. Systematic study of liquidus phase relations in olivine melilitite + H_2O + CO_2 at high pressures and petrogenesis of an olivine melilitite magma. *Contrib. Mineral. Petrol.* **61,** 141–162 (1977).
22. Green, D., Nicholls, I., Viljoen, M. & Viljoen, R. Experimental demonstration of the existence of peridotic liquids in earliest Archean magmatism. *Geology* **3,** 11–14 (1975).
23. Mibe, K. *et al.* Second critical endpoint in the peridotite–H_2O system. *J. Geophys. Res.* **112,** B03201, doi:10.1029/2005JB004125 (2007).
24. Kessel, R., Ulmer, P., Pettke, T., Schmidt, M. W. & Thompson, A. B. The water–basalt system at 4 to 6 GPa: phase relations and second critical endpoint in a K-free eclogite at 700 to 1400 °C. *Earth Planet. Sci. Lett.* **237,** 873–892 (2005).
25. Kovács, I. *et al.* Quantitative absorbance spectroscopy with unpolarized light, part II: experimental evaluation and development of a protocol for quantitative analysis of mineral IR spectra. *Am. Mineral.* **93,** 765–778 (2008).
26. Bell, D. R., Ihinger, P. D. & Rossman, G. R. Quantitative analysis of trace OH in garnet and pyroxenes. *Am. Mineral.* **80,** 465–474 (1995).
27. Bell, D. R., Rossman, G. R., Maldener, J., Endisch, D. & Rauch, F. Hydroxide in olivine: a quantitative determination of the absolute amount and calibration of the IR spectrum. *J. Geophys. Res. B* **108,** 2105, doi:10.1029/2001JB000679 (2003).
28. Niida, K., Green, D. H., Yoshikawa, M. & Eggins, S. M. Dunite channels in the Horoman peridotites, Japan: textural and geochemical constraints on melt/fluid transport through the lithosphere. *Geochim. Cosmochim. Acta* **70,** A445 (2006).
29. Faul, U. H. & Jackson, I. N. S. Diffusion creep of dry, melt-free olivine. *J. Geophys. Res.* **112,** B04204, doi:10.1029/2006JB004586 (2007).
30. Faul, U. H. Melt retention and segregation beneath mid-ocean ridges. *Nature* **410,** 920–923 (2001).

Supplementary Information is linked to the online version of the paper at www.nature.com/nature.

Acknowledgements We thank H. St C. O'Neill, J. Hermann and G. M. Yaxley for discussions, and F. Brink for comprehensive support at scanning electron microscopy (SEM) facilities. We appreciate the help of J. Blundy in the revision of the original manuscript. This research was supported by Australian Research Council grants to D.H.G., and to G. M. Yaxley and D.H.G. I.K. was supported by an A. E. Ringwood Memorial Scholarship, an Australian International Postgraduate Research Scholarship and a Marie Curie International Reintegration Grant (NAMS-230937). A.R. was supported by an Australian National University PhD Scholarship.

Author Contributions D.H.G. initiated and planned the project, and made most of the SEM micro-analyses. W.O.H. carried out the high-pressure experimental work and prepared the experimental charges for SEM analysis. A.R. did some 6 GPa experiments, assisted in SEM analyses and compiled all the analyses. I.K. prepared the thin sections for FTIR analyses, performed the FTIR spectroscopy and processed the data. All authors contributed to the writing of the manuscript.

Author Information Reprints and permissions information is available at www.nature.com/reprints. The authors declare no competing financial interests. Readers are welcome to comment on the online version of this article at www.nature.com/nature. Correspondence and requests for materials should be addressed to D.H.G. (David.H.Green@utas.edu.au).

METHODS

Identification of quenched hydrous silicate melt and of quenched aqueous vapour phase. The diagnostic criterion for quenched hydrous silicate melt is the presence of interstitial patches (interserts) of acicular or lath-shaped crystals of amphibole (and/or quench clinopyroxene), mica and glass, all with Mg number (Mg#) of about 70–85, within the lherzolite and 'melt trap' layers (Supplementary Fig. 2). Conversely, the absence of such intersertal textures and iron-enriched quench phases, together with the presence of porous texture, planes of fluid inclusions in olivine, and stability of hydrous pargasite or phlogopite with Mg# similar to or greater than olivine, is diagnostic of subsolidus conditions and the presence of an aqueous vapour phase. The vapour phase at high pressure dissolves significant oxides, and on quenching may give rise to thin films and coatings of silica-rich glass. In subsolidus experiments with high water content (more than 5 wt%), experimental charges are friable or disaggregated. When observed with scanning electron microscopy (SEM), these samples have euhedral olivine or pyroxene crystals coated with fragmented glass 'froth' or with films of silicate glass, and uncommon rosettes of quench carbonate (Supplementary Fig. 1). These textures are indicative of vapour-phase quench.

We prepared compositions HZ1 and HZ2 (Table 1) by sintering appropriate proportions of high-purity oxides (Si, Ti, Al) or carbonates (Ca, Na, K), then adding Fe as fayalite, and Mg as either MgO (dry mix, to give anhydrous mix A) or $Mg(OH)_2$, (to give mix B, 14.5 wt% H_2O), as in ref. 15. By mixing A and B in appropriate proportions, 100-mg batches with water content 0.073–7.25 wt% H_2O were prepared as experimental starting mixes. In addition, we prepared[17] two starting mixes with about 0.3 and 0.05 wt% H_2O by synthesizing pargasite lherzolite from mix A + 1 wt% H_2O at 1.5 GPa, 950 °C, and from mix A + 0.5 wt% H_2O at 3 GPa, 950 °C. We drove off excess water by heating at 200 °C.

We carried out experiments in half-inch (1.27-cm) piston-cylinder apparatuses at the Research School of Earth Sciences of the Australian National University (ANU) at pressures of 1.5–6.0 GPa and temperatures of 840–1,450 °C for 4.5 h to 7 days, with longer run times used for lower temperature and particularly for 'dry' experiments (Supplementary Tables 3 and 4). We used Au or Ag capsules in lower-temperature experiments and AuPd double capsules at higher temperatures. We used pressed-salt (NaCl) external furnace sleeves with inner MgO-ceramic spacers as the pressure media, and graphite heaters. We controlled the temperature to ±10 °C using a Eurotherm 904 controller and type B thermocouple (Pt94Rh6/Pt70Rh30). From temperature profiling of the furnace assembly, both thermocouple and sample lie within the 'hotspot' of the graphite heater so that sample and thermocouple temperatures are equated.

The use of 'melt traps' and monomineralic layers. As a key aspect of the study was the detection and analysis of near-solidus melts, and/or the segregation of fluid and trapping of fluid-phase quench, we evaluated several techniques for 'melt traps'. Initially, we used layers of carbon spheres with variable water content and temperatures of 1,000 °C–1,075 °C, 2.5 GPa. The carbon spheres added complexity by introducing a C–O–H fluid, which became reduced and CH_4-rich with time, stabilizing pargasite in place of melt in experiments at 1,050 °C and 1,075 °C.

To avoid these effects, we used layers of crushed San Carlos olivine ($Fo_{90–92}$) at both ends of the capsule in other experiments. In these experiments, we observed fluid inclusions and pore space or quenched silicate melt within the olivine melt trap. A third technique used thin (approximately 100 μm) olivine disks placed in the centre of the capsule between layers of lherzolite + H_2O mixes. This enabled cracking and re-healing of olivine with capture and trapping of fluid inclusions within the olivine disk. By preparing doubly polished thin sections with thicknesses 37–124 μm from experimental charges, we demonstrated that quantitative measurements of water in olivine could be achieved from both olivine disks and polycrystalline olivine layers by FTIR. In experiments with HZ1 composition and olivine disks or layers, the addition of olivine with Mg# of about 90 does not alter ratios of the oxides H_2O, K_2O, Na_2O, CaO, Al_2O_3 or TiO_2, which are important for issues of vapour phase composition and clinopyroxene or pargasite compositions. With demonstration of the suitability of olivine layers for FTIR analyses, we carried out further experiments using alternately high-alumina and low-alumina orthopyroxenes and clinopyroxenes as sensor layers for water in NAMs. The use of orthopyroxene or clinopyroxene mineral layers for the purpose of measuring water content adds a complication, in that these layers react with the phases of the lherzolite layer. We used the experiments with pyroxene layers only for the FTIR estimation of water-in-pyroxene and not in the discussion of phase relations of the lherzolite HZ1 composition.

Analytical methods. We mounted, polished and carbon-coated the recovered capsules from the assemblies. We examined the run products (phase assemblages) by SEM and energy dispersive spectrometry (EDS), using a JEOL 6400 SEM with energy-dispersive X-ray analysis (EDS) facility or a Hitachi 4300 field emission SEM. All facilities are housed in the Electron Microscopy Unit of the ANU. We used an accelerating voltage of 15 kV, a beam current of 1 nA with a fully focused beam, and a counting time of 120 s for phase analyses, except for analyses of 'decorated' fluid inclusion cavities, for which we performed area scans of appropriate size (usually less than 20 × 30 μm). We used mineral standards produced by Astimex Scientific to standardize mineral and glass analyses, and obtained averages of multiple analyses of each mineral phase and quenched liquid compositions. Detection limits are about 0.10 wt% for K_2O, TiO_2 and MnO, and about 0.15 wt% for Na_2O and Cr_2O_3. In addition to spot analyses of the mineral phases in experiments, the presence of interserts of melt within the olivine layer melt-traps enabled analysis of quenched melt. We used area-scan methods to analyse quench aggregates and plotted Mg# versus oxides to estimate quenched melt composition. For example, at 2.5 GPa, 1,025 °C, with 1.45 and 0.3 wt% H_2O, melts are olivine-rich basanite (about 6% melting) and olivine nephelinite to melilitite (about 1% melting) respectively, assuming approximately 25 wt% H_2O dissolved in the melts.

We obtained excellent infrared spectra from the olivine disk fragments, the olivine layers and the lherzolite layers, including recognition of specific pargasite or phlogopite spectra where these phases were present. We excluded epoxy resin in the preparation of doubly polished thin sections. We kept samples in an oven at 90 °C before analysis. We used a Bruker IFS-28 infrared spectrometer mounted with an A590 Bruker infrared microscope supplied with a nitrogen-cooled mercury cadmium telluride detector for infrared analysis, including use of a KBr beam splitter. We recorded spectra in the range 600–5,000 cm^{-1}. The spectra have a resolution of 4 cm^{-1}. We made analyses with a circular aperture of 40–80 mm diameter, and we continuously flushed the box surrounding the microscope stage, in which we placed silica gel, with nitrogen to minimize water-vapour background. We processed spectra using the OPUS 6.0 software (Bruker). In most cases, we subtracted the background using the interactive rubber-band correction of the OPUS software and in some instances (for olivine) drew it manually. We obtained the integrated intensities of the main absorption bands with the Integration tool of the OPUS software, using appropriate integration limits. We calculated the total integrated absorbance from 9–20 spectra using the method of ref. 25. For the quantification of the integrated absorbances, we used the calibration factors of refs 26 and 27 for ease of comparison with other studies. By these methods we measured water content in the sensor layers of olivine, olivine + orthopyroxene and clinopyroxene + orthopyroxene, and thus obtained olivine/orthopyroxene and orthopyroxene/clinopyroxene partition coefficients directly from experiments in which we also characterized melt, pargasite and/or vapour in the lherzolite layer. We assumed water content in pargasite from stoichiometry (2 wt%), and we used a water content of about 30 wt% in olivine-rich magmas at vapour-saturation at 2.5–3.5 GPa (refs 20–24). Thus we calculated olivine/pargasite, olivine/melt, and so on. We estimated the water content of residual peridotite and peridotite/melt using the same modal mineralogy as ref. 1 to facilitate comparison with literature.